Journal of Constructional Steel Research 67 (2011) 1719–1732

Contents lists available at ScienceDirect

Journal of Constructional Steel Research

Nonlinear analysis of concrete-filled square stainless steel stub columns under axial compression

Zhong Tao [a,*], Brian Uy [a], Fei-Yu Liao [b,c], Lin-Hai Han [b]

[a] Civionics Research Centre, University of Western Sydney, Penrith, NSW 2751, Australia
[b] Department of Civil Engineering, Tsinghua University, Beijing, 100084, China
[c] College of Transportation, Fujian Agriculture and Forestry University, Fuzhou, Fujian, 350002, China

ARTICLE INFO

Article history:
Received 7 January 2011
Accepted 28 April 2011
Available online 31 May 2011

Keywords:
Concrete-filled steel tubes
Stainless steel
Stub columns
Axial compression
Nonlinear analysis
Finite element
Strength
Parametric analysis

ABSTRACT

Concrete-filled stainless steel tubes (CFSST) can be considered as a new and innovative kind of composite construction technique, and have the potential to be used extensively in civil engineering. This paper employs a nonlinear analysis of square CFSST stub columns under axial compression. A three-dimensional nonlinear finite element (FE) model is developed using ABAQUS, where nonlinear material behaviour, enhanced strength corner properties of steel, and initial geometric imperfections are included. Close agreement is achieved between the test and FE results in terms of load-deformation response and ultimate strength. In light of the numerical results, the behaviour of stainless steel composite columns is compared with that of carbon steel composite columns. A simple model is proposed to calculate the ultimate strength of square CFSST stub columns.

1. Introduction

In recent times, there has been an accelerating interest in the use of stainless steel in construction throughout the world [1,2]. This is attributed to the fact that stainless steel is extremely durable, has greater corrosion resistance and improved fire resistance, and is easily maintained. Several previous projects to have utilised stainless steel include the 300 m tall St Louis, Missouri, USA (1966), the 81 m tall Parliament House Flag Pole in Canberra, Australia (1988), and the Hearst Tower at 959 Eight Avenue, New York City, USA (2006) [3]. A more recent structural use of stainless steel is in the Stonecutters bridge in Hong Kong which was completed in 2009 [3]. This bridge consists of two 298 m high towers with their upper parts comprising of a stainless steel section filled with concrete. Due to the merits of stainless steel, it is evident that it has a very important role to play in the future design of structures, particularly when architects and structural engineers become more cognisant of the need for life cycle costing [4].

Compared with mild carbon steel, however, the structural use of stainless steel is still in its infancy. In spite of the benefits which stainless steel can offer, its application in structures has been greatly inhibited by its initial high cost [1,2]. With a cost of about 3–5 times that of mild carbon steel, it is evident that more efforts should be made to make the optimum use of its properties.

A promising method to better utilise and compensate for the high cost of adopting stainless steel is to use hollow sections filled with concrete. It is a natural progression since concrete-filled steel tubular (CFST) columns using carbon steel material have been studied and applied in engineering practise for over one century. It has been shown that the composite columns combine the advantages of both steel and concrete, and thus provide not only an increase in the load-carrying capacity but also rapid construction, and additional cost saving [5,6]. Hence, it is expected that a CFST column fabricated with stainless steel will ideally combine the advantages of both stainless steel and conventional concrete-filled carbon steel tubes. In this case, the amount of stainless steel used can be greatly reduced by concrete filling. This has been validated by some recent tests performed by several researchers [7–10].

So far, numerous investigations have been conducted on the behaviour of carbon steel CFST columns [6], whilst research on concrete-filled stainless steel tubular (CFSST) columns is still quite limited. Using a cross-sectional analysis method based on the approach presented in [11], a simple mechanics model was developed by Roufegarinejad et al. [12] to analyse the moment-curvature response of square CFSST sections. Up to now, a total of over 100 tests have been conducted on short and slender CFSST columns in [7–10], which demonstrated that the performance of CFSST columns was quite good, even when stiffened thin-walled tubes were used. Finite

* Corresponding author. Tel.: +61 2 4736 0064; fax: +61 2 4736 0054.
E-mail address: z.tao@uws.edu.au (Z. Tao).

0143-974X/$ – see front matter © 2011 Elsevier Ltd. All rights reserved.
doi:10.1016/j.jcsr.2011.04.012

Nomenclature

A_c	Cross-sectional area of concrete
A_s	Cross-sectional area of steel
B	Width of the square steel tube
E_0	Initial elastic modulus of stainless steel
f_c'	Cylinder compressive strength of concrete
f_{ck}	Characteristic concrete strength ($=0.67f_{cu}$ for normal strength concrete)
f_{cu}	Compressive cube strength of concrete
f_y	Yield strength of carbon steel
L	Specimen length
n	Strain-hardening exponent
N	Axial load
N_u	Ultimate strength
N_{uc}	FE predicted ultimate strength
p	Interaction stress between the steel tube and concrete
p_{ave}	Average interaction stress
r_i	Internal corner radius of the cold-formed section
t	Wall thickness of the steel tube
α	Steel ratio ($=A_s/A_c$)
ε	Strain
ε_{cu}	Ultimate axial strain
σ	Stress
$\sigma_{0.2}$	0.2% proof stress of stainless steel
$\sigma_{0.2,a}$	Average nominal yield strength
$\sigma_{0.2,c}$	0.2% proof stress of corner material
ω_0	Amplitude of initial geometric imperfections
ξ	Confinement factor

element (FE) analyses using the commercial software ABAQUS were performed by Ellobody and Young [13] and Ellobody [15] to analyse the nonlinear behaviour of square CFSST stub columns and thin-walled stiffened CFSST stub columns, respectively. However, only measured stress–strain curves for the stainless steel were used in the FE models presented in [13,15]. More recently, Hassanein [16] carried out a numerical modelling of concrete-filled lean duplex thin-walled stainless steel tubular stub columns by using the stress–strain relation proposed by Rasmussen [17] to define the material behaviour of lean duplex stainless steel. The enhanced strength corner properties of stainless steel and initial geometric imperfections have not been included in the FE model presented by Hassanein [16]. From the literature review, it seems that more research needs to be carried out to recognise the possible behaviour differences between stainless steel and carbon steel CFST columns. Only by doing so can rational design methods be put forward to better design CFSST columns.

This paper aims to perform a nonlinear analysis of square CFSST stub columns under axial compression. Previous available test results are used in the present study to establish consistent FE modelling technique using ABAQUS [18], where nonlinear material behaviour, enhanced strength corner properties of steel, and initial geometric imperfections are included. Using the FE model, the behaviour of CFSST columns is compared with that of carbon steel composite columns. A series of parametric studies is further carried out to investigate the effects of different parameters on the behaviour of CFSST columns. A simple model is proposed to calculate the section capacities of the stainless steel composite columns.

2. Finite element model and verification

2.1. General

ABAQUS software package was employed throughout the FE analysis. The steel tube was simulated by using 4-node shell elements with reduced integration (S4R). The concrete core was modelled using 8-node brick elements (C3D8R), with three translation degrees of freedom at each node. A mesh convergence study was performed to identify an appropriate mesh density to achieve reliable results with reasonable computation times. The adopted FE mesh for a typical column is shown in Fig. 1.

In the past, surface-based interaction with a contact pressure model in the normal direction and a Coulomb friction model in the tangential directions to the surface between the steel tube and core concrete, has been successfully used to simulate carbon steel CFST columns [19,20]. A friction coefficient of 0.25 was used in those models. Since the surface of stainless steel is covered with a chemically stable chromium oxide for good corrosion resistance, the friction coefficient and bond behaviour between the steel tube and

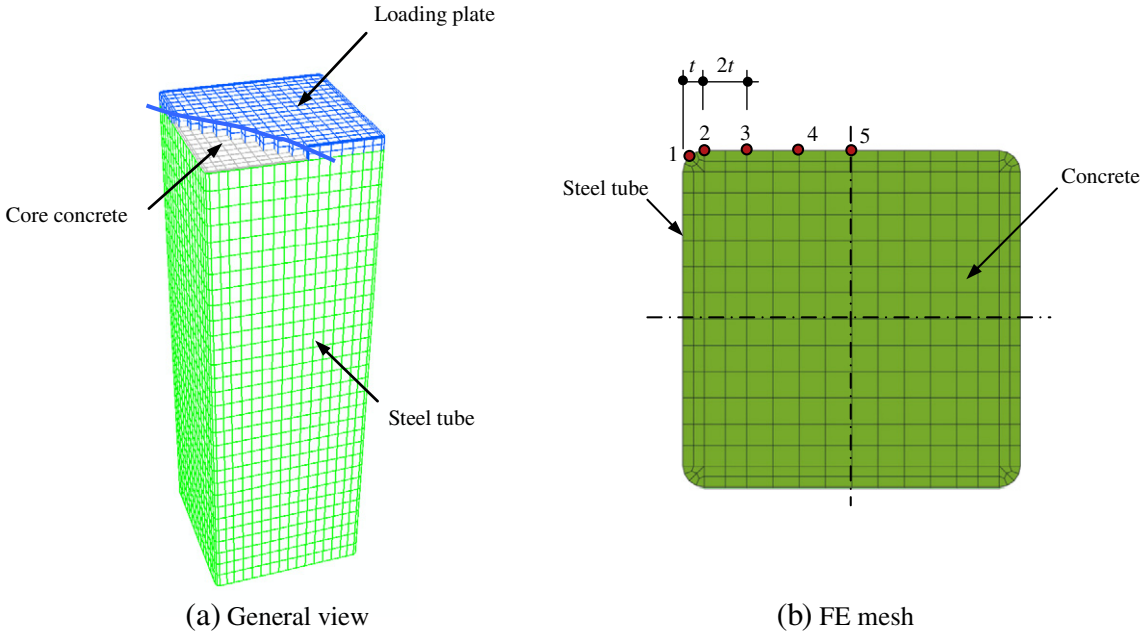

(a) General view (b) FE mesh

Fig. 1. Typical finite element model.

core concrete are likely to be different compared with that in conventional carbon steel CFST columns. Since no bond tests have been carried out so far to study this mechanism, and the bond behaviour is expected to have very minor influence on the performance of a stub column, the same steel tube–concrete interface model presented by Han et al. [19] is used in the following analysis.

Loading was applied in a displacement control mode at the top of a stub column to simulate the axial loading condition. The ends of the stub column were fixed against all degrees of freedom except for the vertical displacement at the top end. To accelerate convergence, a top end plate was added as shown in Fig. 1(a). Due to the nonlinear nature of the modelling, the well-known Newton–Raphson incremental-iterative solution method was used in the analysis.

2.2. Material modelling

2.2.1. Stainless steel

To develop a suitable model for stainless steel is very crucial in modelling CFSST columns since the material behaviour of stainless steel is quite different from that of carbon steel. It is well known that the nonlinear stress (σ)–strain (ε) curves of stainless steel are of a "roundhouse" type [17,22]. To describe this material stress–strain behaviour, the Ramberg–Osgood relationship is often used for stainless steel:

$$\varepsilon = \frac{\sigma}{E_0} + 0.002\left(\frac{\sigma}{\sigma_{0.2}}\right)^n \tag{1}$$

in which E_0 is the initial elastic modulus, and $\sigma_{0.2}$ is the 0.2% proof stress. n is the strain-hardening exponent determined by $\sigma_{0.2}$ and the 0.01% proof stress $\sigma_{0.01}$:

$$n = \frac{ln(20)}{ln(\sigma_{0.2}/\sigma_{0.01})}. \tag{2}$$

It was found that Eq. (1) gives accurate predictions of stainless steel stress–strain behaviour up to the 0.2% proof stress $\sigma_{0.2}$, but the predictions become seriously inaccurate when the stresses are beyond that level [17]. To address this issue, attempts have been made by several researchers to model the nominal stress–strain behaviour of stainless steel at high strains.

A full-range stress–strain relationship was proposed by Rasmussen [17], in which the Ramberg–Osgood expression [Eq. (1)] was used for the range up to the 0.2% proof stress, and a new expression given by Eq. (3) is used for higher strains.

$$\varepsilon = \frac{\sigma-\sigma_{0.2}}{E_{0.2}} + \varepsilon_u\left(\frac{\sigma-\sigma_{0.2}}{\sigma_u-\sigma_{0.2}}\right)^m + \varepsilon_{0.2}, \sigma > \sigma_{0.2} \tag{3}$$

in which

$$E_{0.2} = \frac{E_0}{1 + 0.002n/e} \tag{4}$$

$$e = \frac{\sigma_{0.2}}{E_0} \tag{5}$$

$$\frac{\sigma_{0.2}}{\sigma_u} = \frac{0.2 + 185e}{1-0.0375(n-5)} \tag{6}$$

$$\varepsilon_u = 1-\frac{\sigma_{0.2}}{\sigma_u} \tag{7}$$

$$m = 1 + 3.5\frac{\sigma_{0.2}}{\sigma_u} \tag{8}$$

$$\varepsilon_{0.2} = \frac{\sigma_{0.2}}{E_0} + 0.002. \tag{9}$$

As can be seen, only the three basic Ramberg–Osgood parameters (E_0, $\sigma_{0.2}$, and n) are needed in the Rasmussen's model to determine the full-range stress–strain relationship.

Gardner and Nethercot [21] proposed a model in which Eq. (10) is used for the range beyond the 0.2% proof stress, and Eq. (1) continues to apply for stresses up to $\sigma_{0.2}$.

$$\varepsilon = \frac{\sigma-\sigma_{0.2}}{E_{0.2}} + \left[0.008-\frac{\sigma_{1.0}-\sigma_{0.2}}{E_{0.2}}\right]\left(\frac{\sigma-\sigma_{0.2}}{\sigma_{1.0}-\sigma_{0.2}}\right)^{n'_{0.2,1.0}} + \varepsilon_{0.2}, \sigma > \sigma_{0.2} \tag{10}$$

where $n'_{0.2,\,1.0}$ is the strain-hardening coefficient representing a curve that passes through $\sigma_{0.2}$ and the 1.0% proof stress $\sigma_{1.0}$. It should be noted that no expressions have been recommended by Gardner and Nethercot [21] to predict the values of $\sigma_{1.0}$ and $n'_{0.2,\,1.0}$. Thus, they can be determined from measured stress–strain curves.

Quach et al. [22] realised that the Rasmussen's model provides excellent predictions for tension coupon tests in general, but underestimates the nominal stresses at strains $\varepsilon > \varepsilon_{0.2}$ for most compression coupon tests (see Fig. 2). As far as the Gardner and Nethercot's model is concerned, Quach et al. [22] pointed out that this model presents an accurate expression for the nominal stress–strain curves for both tension and compression, up to relatively high strains of general structural interest, but their expression may not provide accurate predictions for higher strains likely to be encountered during corner bending in the cold-forming process of stainless steel sections.

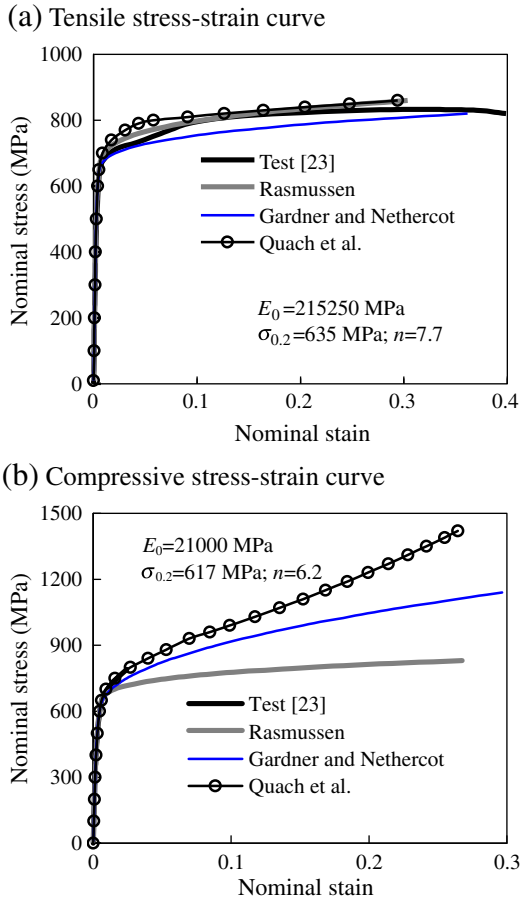

Fig. 2. Comparisons of model predictions with measured nominal stress–strain curves [23].

Quach et al. [22] proposed a three-stage nominal stress–strain model that can be used over the full ranges of both tensile and compressive strains. In this model, the Ramberg–Osgood expression [Eq. (1)] was used for the first range up to the 0.2% proof stress, and the expressions for the second and third ranges are as follows:

$$\varepsilon = \frac{\sigma-\sigma_{0.2}}{E_{0.2}} + \left[0.008 + (\sigma_{1.0}-\sigma_{0.2})\left(\frac{1}{E_0}-\frac{1}{E_{0.2}}\right)\right] \times \left(\frac{\sigma-\sigma_{0.2}}{\sigma_{1.0}-\sigma_{0.2}}\right)^{n'_{0.2,1.0}} + \varepsilon_{0.2}, \sigma_{0.2} < \sigma \leq \sigma_{2.0} \tag{11a}$$

$$\varepsilon = \frac{\sigma-a}{b \mp \sigma}, \sigma > \sigma_{2.0} \tag{11b}$$

where the upper sign corresponds to tension, and the lower sign to compression; $\sigma_{2.0}$ is the 2.0% proof stress; and a and b are constants presented by Quach et al. [22]. It should be mentioned that empirical expressions have been proposed by Quach et al. [22] to calculate $\sigma_{1.0}$, $\sigma_{2.0}$ and $n'_{0.2,\ 1.0}$ used in Eq. (11). Therefore, the Quach et al.'s model can also be defined using only the three basic Ramberg–Osgood parameters.

As pointed out by Quach et al. [22], it seems that the Rasmussen's model is more suitable for predicting the nominal stress–strain behaviour of stainless steel in tension other than in compression. ABAQUS, however, requires that the material stress–strain relationship is defined only in terms of true stress σ_{true} and logarithmic plastic true strain ε^{pl}_{true}. The values of σ_{true} and ε^{pl}_{true} can be converted from the nominal (engineering) stress (σ) and strain (ε) in tension using Eqs. (12) and (13), respectively.

$$\sigma_{true} = \sigma(1+\varepsilon) \tag{12}$$

$$\varepsilon^{pl}_{true} = ln(1+\varepsilon) - \frac{\sigma_{true}}{E_0} \tag{13}$$

Generally, the true stress–strain curves for stainless steel in tension coincide with the curves in compression [22]. Fig. 3 compares the three stress–strain models' predictions in terms of true stress–strain relationship. As can be seen, there is no significant difference among the three model predictions. The predictions using the Rasmussen's model agree well with those based on the Quach et al.'s model. For simplicity considerations, Rasmussen's model [Eqs. (1) and (3)] was used in this paper, and the nominal stress–strain relationship was thus converted to a true stress–strain relationship according to Eqs. (12) and (13).

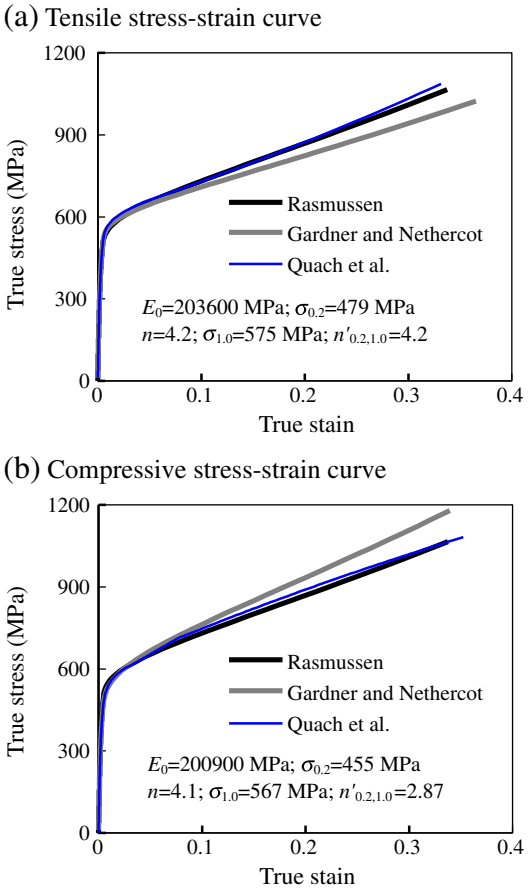

Fig. 3. Typical true stress–strain curves for stainless steel.

2.2.2. Mild carbon steel

Carbon steel CFST stub columns were also analysed in this paper for comparison purposes. An idealised multi-linear stress–strain model developed by Abdel-Rahman and Sivakumaran [24] for cold-formed carbon steel tubes was used in this paper. This model was also used by Han et al. [19]. The yield surface was defined by the Von-Mises yield criterion, and the plastic deformations were determined by the Prandtl-Reuss flow rule.

2.2.3. Confined concrete

The damage plasticity model provided in the material library of ABAQUS [18] was used for the core concrete in the analytical model. By using the finite element method, strength enhancement at the state of triaxial loading can be achieved by the definition of the yielding surface, and the description of the plastic behaviour coming from the equivalent stress–strain relationship of the confined concrete. To simulate the plastic behaviour of the core concrete in CFSTs under compression, an equivalent stress–strain model has been proposed by Han et al. [19]:

$$y = \begin{cases} 2\cdot x - x^2 & (x \leq 1) \\ \dfrac{x}{\beta_0\cdot(x-1)^{\eta}+x} & (x>1) \end{cases} \tag{14}$$

where $x=\varepsilon/\varepsilon_0$, $y=\sigma/f'_c$; f'_c is the cylinder compressive strength of concrete; ε_0, β_0, η are model parameters, and related to the confinement factor ξ used to describe the increase in plastic behaviour due to the passive confinement of the steel tube. This factor ξ was defined as $\xi=(A_s f_y/A_c f_{ck})=\alpha(f_y/f_{ck})$, in which $\alpha=A_s/A_c$ is the steel ratio, A_s and A_c are the cross-sectional areas of the steel and core concrete respectively, f_y is the yield strength of carbon steel, f_{ck} is the characteristic strength of the concrete equal to $0.67f_{cu}$ for normal strength concrete, and f_{cu} is the cube strength of concrete.

The above stress–strain model has been used successfully to simulate conventional carbon steel CFST columns under compression, shearing, bending, torsion and combined loading by the authors. It is expected that the passive confinement of concrete by the stainless steel tube should not significantly differ from that of carbon steel tubes. Thus, this model was also used in simulating the CFSST columns, in which the yield strength (f_y) for carbon steel was replaced by the 0.2% proof stress ($\sigma_{0.2}$) for stainless steel.

2.3. Corner material properties

Currently, the majority of stainless steel square or rectangular hollow sections are formed by cold rolling. Therefore, only CFSST

columns fabricated from cold-formed steel sections are investigated in this paper. Similar to carbon steel, there is significant strength enhancement at the corner regions of cold-formed sections, and this effect is even more pronounced than carbon steel [25,26]. It is reported that the strength enhancement is commonly between 20% and 100% in terms of 0.2% proof strength compared with the flat regions [27].

Lecce and Rasmussen [26] compared three different models in predicting the strength enhancements induced during cold forming of stainless steel sections. It was found that the two models proposed by Ashraf et al. [25] and AS/NZS 4673 [14] give generally good predictions compared with test results conducted by Lecce and Rasmussen [26], although all models underestimate the corner yield strengths by more than 14% on average. It was also pointed out by Lecce and Rasmussen [26] that the model presented in AS/NZS 4673 gives more consistent predictions with a smaller standard deviation, thus this model was used in [26] to carried out a FE analysis. However, for a cold-formed section, strength enhancement is not only achieved at the corner regions but also extend a distance to the flat regions [28,29]. This effect was not considered by Lecce and Rasmussen [26].

To account for the above effect, Ashraf et al.'s model [25] was further revised with minor modifications by Cruise and Gardner [29] using more published test data. The new model is expressed by Eq. (15) to predict the enhanced corner material strength.

$$\sigma_{0.2,c} = \frac{1.673\sigma_{0.2,v}}{(r_i/t)^{0.126}} \tag{15}$$

where $\sigma_{0.2,c}$ and $\sigma_{0.2,v}$ are the 0.2% proof stresses of the corner material and the virgin material, respectively; r_i is the internal corner radius; t is the thickness of the cross-section.

Eq. (15) was used in the current FE modelling to predict the strength enhancement for a region including the corner radius and a distance of $2t$ extending to each flat region [28,29]. Since there is no specific stress–strain model proposed in the literature for corner materials, $\sigma_{0.2,c}$ was used in the aforementioned Rasmussen's model to derive the full stress–strain curves with the same E_0 and n used for the corresponding flat material.

It should be noted that, since the magnitude of the internal corner radius (r_i) was not presented in some previous test reports, an assumed r_i taken as the same magnitude with the thickness of steel tube (t) is adopted in these cases.

2.4. Initial imperfections

The shape of local initial imperfections is often assumed to be the same as that of the expected local buckling shape. According to this principle, the shape of the imperfections for steel plates in a square CFST stub column was assumed by Tao et al. [20] to be of the following form (Fig. 4):

$$\omega = \frac{\omega_0}{4}\left(1-\cos\frac{2\pi x}{B}\right)\left(1-\cos\frac{2\pi y}{B}\right) \tag{16}$$

where x and y are the lateral and axial coordinates, respectively, from one end of the tube; B is the width of the tube; ω_0 is the amplitude of the local imperfections, which was taken as $0.01B$ by Tao et al. [20].

For carbon steel CFST stub columns, the calculated load-deformation curves using the above assumed imperfections were compared with the calculated ones where measured imperfections were used [20]. Satisfactory agreement has been achieved, and all the predicted curves showed good agreement with test results. Since the magnitude of imperfections is likely to be a complex function of the rolling and fabrication process, material and geometrical properties of cross-sections [28], the definition of ω_0 as $0.01B$ may not be suitable for stainless steel cross-sections.

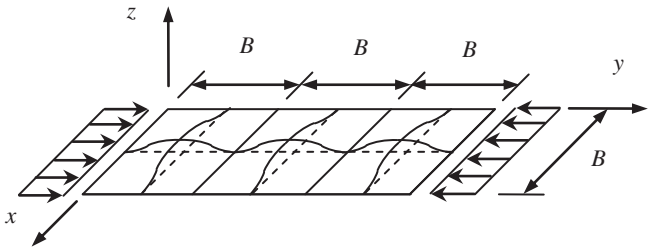

Fig. 4. Local imperfections assumed for square CFST columns [20].

For hollow stainless steel cross-sections, Gardner and Nethercot [27] and Ashraf et al. [28] proposed Eq. (17) for the determination of ω_0:

$$\omega_0 = 0.023(\sigma_{0.2}/\sigma_{cr})t \tag{17}$$

in which σ_{cr} is the elastic critical plate buckling stress. Obviously, the magnitude of ω_0 determined using Eq. (17) is generally much smaller than $0.01B$. Given a simply supported plate element with a width (B) of 150 mm and a thickness (t) of 2 mm, ω_0 will be 0.107 mm according to Eq. (17) if $\sigma_{0.2}$ is taken as 300 MPa. But if ω_0 is taken as $0.01B$, it will be 1.5 mm.

It's worth noting that the imperfection magnitude of $0.01B$ used in [20] was only for thin-walled tubes where four component plates were longitudinally welded in the vertices. This proposed ω_0 was in accordance with experimental measurements reported in [20]. To compare the behaviour of CFSST columns with that of carbon steel CFST columns in this paper, cold-formed carbon steel tubes are expected to be used in the latter. In this case, the value of ω_0 for these tubes is supposed to be smaller than $0.01B$. However, CFST columns are not sensitive to the variation of the imperfection magnitude, as pointed out in Section 4.2 and in [20]. Therefore, $0.01\ B$ will be tentatively used in the following to determine the amplitude of the initial imperfections for carbon steel CFST columns, whilst Eq. (17) will be used to calculate that of CFSST columns. It is recommended to measure initial imperfections for cold-formed carbon steel CFST columns in the future.

2.5. Residual stresses

Membrane stresses and bending residual stresses can be detected in a cold-formed stainless steel member. In general, the effects of bending residual stresses are inherently present in a stress–strain model, and only membrane stresses induced through welding need to be considered in numerical models [28]. Previous investigations by Ashraf et al. [28] and Gardner and Nethercot [27] have shown that the residual stresses cause only a small reduction in initial stiffness but have little influence on the overall load-deformation response for a stainless steel column. A similar conclusion has been reached in the investigation by Ellobody and Young [30], where measured residual stresses were used in the FE modelling.

It is expected that the influence of residual stresses will be further minimised for a CFST column by concrete filling. This beneficial influence has been demonstrated in previous investigations [20,31]. Hence, the residual stresses are not included in the following analysis to improve the computation efficiency.

2.6. Model verification

A comparison between the available test results and FE results was carried out to verify the finite element model. Fig. 5 shows a comparison between the numerical deformed shape and the observation of a typical square CFSST stub column presented by Uy et al. [10]. Fig. 6 compares the predicted axial load (N) versus axial strain (ε) curves with typical measured curves presented previously in [7,8,10]. The dimensions and material properties for the specimens compared are given in Table 1, where L is the specimen length. It is pertinent to note that only part test curves are randomly selected to present herein due to page limitations.

The predicted ultimate strengths (N_{uc}) are compared with those obtained from tests (N_{ue}) in Table 1 and Fig. 7. According to [10], the axial load (N) versus axial strain (ε) curves for CFSST stub columns can be roughly classified into three types, i.e., Type A, Type B and Type C. The classification depends mainly on the confinement of steel tubes to concrete. Type A and Type C are the typical N–ε relationships with a strain-hardening and strain-softening response, respectively, whilst Type B curve decreases after reaching its first peak load, and then the load increases significantly once again. Generally, the maximum loads for Type A and Type B specimens are often associated with very high plastic strains. In [10], if the maximum load or first peak load attained below 1% strain, N_{ue} was taken a same value as the maximum or first peak load; otherwise N_{ue} was defined as the strength corresponding to a maximum strain limit of 1%. For comparison purposes, the same definition of N_{ue} is used in this paper and the corresponding values of N_{ue} for different specimens are given in Table 1. A mean ratio (N_{ue}/N_{uc}) of 1.036 is obtained with a standard deviation of 0.095.

From the above comparisons, it can be found that generally good agreement is obtained between the predicted and test results. Therefore, the FE model described above can be used to conduct further analysis and to compare the behaviour of CFSST stub columns with that of corresponding carbon steel CFST columns.

3. Analysis and discussion

Three typical CFSST stub columns reported previously by Uy et al. [10] are selected herein to conduct behaviour analysis. These specimens are S30-50×3-A (Type A), S30-50×2-A (Type B), and S30-150×3-A (Type C), respectively, as given in Table 1. For comparison purposes, N–ε curves of corresponding carbon steel CFST columns were also computed where f_y of carbon steel was taken as the value of $\sigma_{0.2}$ of stainless steel, and all the other parameters remained the same.

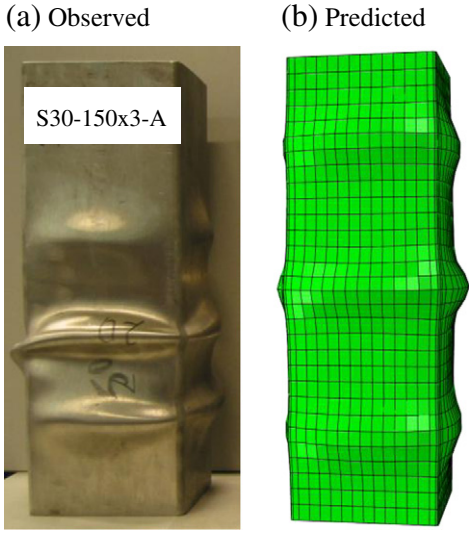

Fig. 5. Comparison of observed and predicted failure modes.

3.1. N–ε curves

Fig. 8 shows the axial load (N)–axial strain (ε) curves for different types of CFSST columns. The axial loads carried by the steel tube and concrete core are also presented in Fig. 8 as a function of ε, respectively. For the Type A or Type B CFSST column, there is no obvious strength decline for the steel tube even up to an axial strain of 0.02. Different from the concrete in the Type A CFSST column, the concrete in the Type B column shows a marked strain-softening behaviour owing to the less efficient confinement provided by the steel tube. At a later stage, the hardening effect of the steel and the increasing confinement to the concrete compensate the strain-softening of the concrete, and lead to the second aforementioned ascending branch of the Type B curve as shown in Fig. 8(b). For the Type C curve, the load carried by the steel tube decreases significantly after reaching its peak load. This is owing to the influence of the local buckling of the thin-walled steel tube. Meanwhile, the concrete exhibits substantial strain-softening with decreased confinement. Clearly, the higher the confinement of the steel tube, the more ductile the column is.

It can also be found from Fig. 8 that a CFSST column has a higher ultimate strength (N_{uc}) compared with its carbon steel counterpart. However, this strength increase is less significant when the type of the curve changes from Type A to Type B and then to Type C. For the Type A and Type B columns, compared with their carbon steel counterparts, the strength increases of the CFSSTs are 12.8% and 2.4%, respectively. But for the Type C CFSST column, its strength is virtually the same as that of its carbon steel counterpart. The strength enhancement for the Type A and Type B CFSST columns is mainly attributed to the relatively strong strain-hardening of stainless steel and enhanced strength at corner regions. But the strain-hardening has not yet begun for the Type C CFSST column when the peak load is reached with a corresponding ultimate axial strain $\varepsilon_{cu} = 2858\ \mu\varepsilon$. The nominal yield strain of the stainless steel ($\varepsilon_{0.2}$) for this specimen is 3391 με, which is larger than the value of ε_{cu}. Obviously, the material behaviour of stainless steel has not yet been fully utilised for the Type C column when reaching its peak load. However, even though the strain-hardening effect may not be effective in increasing the ultimate strength for Type C CFSST columns, it can still increase the residual strength of a column after experienced large axial deformation. This increased residual strength may be crucial to the survival of a structure when subjected to extreme loads.

As mentioned earlier, the nonlinear stress–strain curve of stainless steel is of the "roundhouse" type [22]. To illustrate this influence, the initial curve of the Type A column presented in Fig. 8 is depicted in Fig. 9. Since stainless steel shows gradual yielding behaviour, the value of ε_{cu} for a CFSST column is larger than the corresponding ε_{cu}' of the carbon steel composite columns. But the influence of the nonlinearity of stainless steel is greatly reduced by the presence of the infill concrete, especially for Type B and Type C columns with less strength contributed by the steel tube. As the curve of the CFSST column changes from Type A to Type B and then to Type C, ε_{cu} gets closer and closer to its corresponding ε_{cu}', as shown in Fig. 8.

3.2. Interaction between the steel tube and concrete

From the comparison shown in Fig. 8, it seems that the steel type has very minor influence on the N–ε curves of the concrete. To further clarify this, five different points around the perimeter of the concrete core for the specimen S30-50×3-A are selected to illustrate the

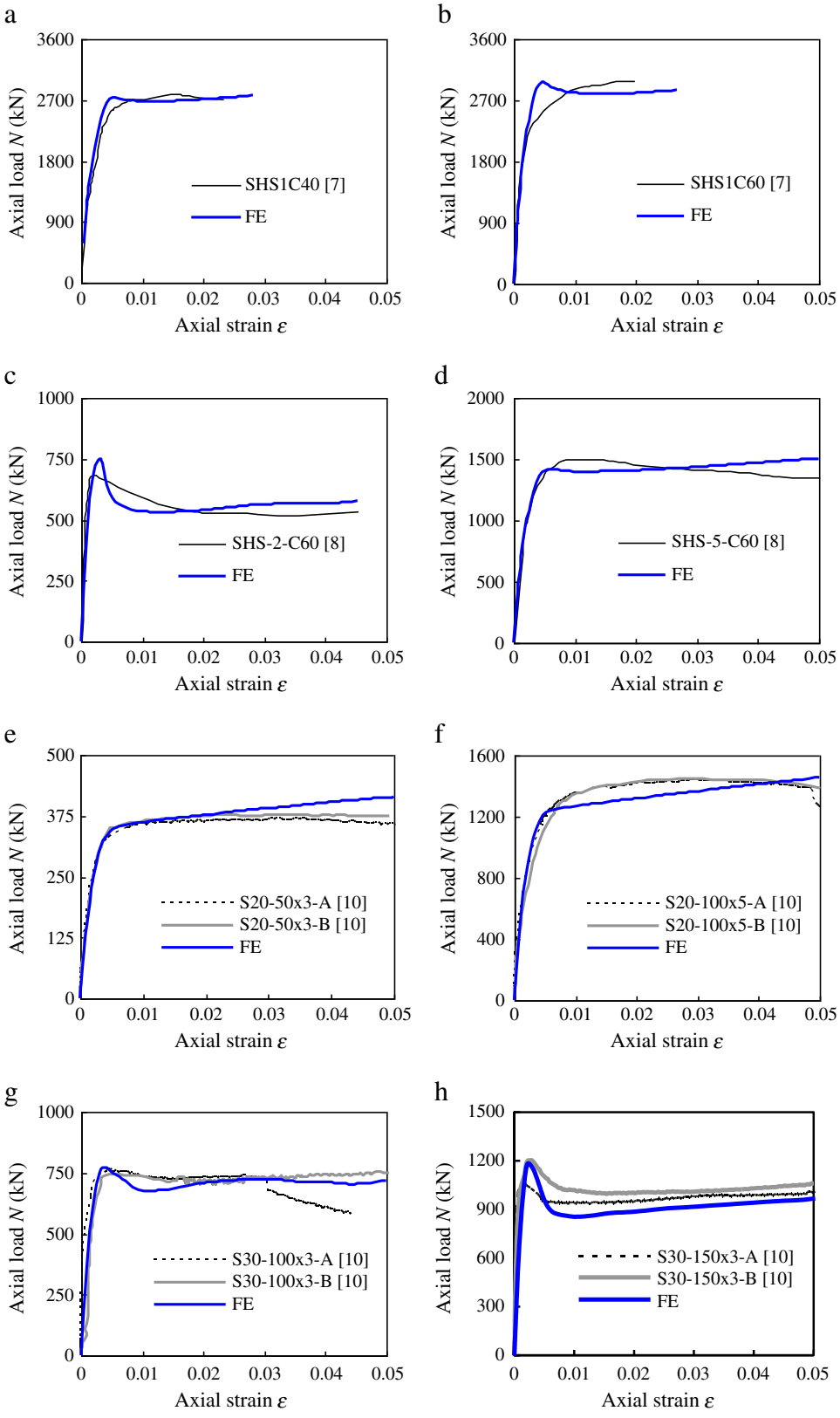

Fig. 6. Comparison of predicted versus experimental axial load-axial strain curves.

interaction stress (p) between the steel tube and concrete. The confinement of the steel tube to the concrete is directly associated with the magnitude and distribution of p. The positions of these points are shown in Fig. 1 (b), where Point 1 is the midpoint of the corner arc ($r_i = t$), Point 2 is at the junction of the corner and the flat regions, Point 3 is at a distance of $2t$ from Point 2 which is the end of the corner strength enhancement region, Point 5 is the midpoint of the flat region, and Point 4 is in the middle of Point 3 and Point 5.

Table 1
Test data of concrete-filled square stainless steel tubular stub columns.

No.	Specimen label	$B\times t\times L$ (mm)	r_i	E_0 (MPa)	$\sigma_{0.2}$ (MPa)	n	f_c' (MPa)	N_{ue} (kN)	N_{uc} (kN)	N_{ue}/N_{uc}	Test data source
1	S20-50×2-A	51×1.81×150	–	205,100	353	10.4	21.5	234	201	1.16	[10]
2	S20-50×2-B	51×1.81×150	–	205,100	353	10.4	21.5	243	201	1.21	
3	S20-50×3-A	51×2.85×150	–	207,900	440	8.2	21.5	358	362	0.99	
4	S20-50×3-B	51×2.85×150	–	207,900	440	8.2	21.5	364	362	1.01	
5	S20-100×3-A	100×2.85×300	–	195,700	358	8.3	21.5	705	736	0.96	
6	S20-100×3-B	100×2.85×300	–	195,700	358	8.3	21.5	716	736	0.97	
7	S20-100×5-A	101×5.05×300	–	202,100	435	7.0	21.5	1352	1268	1.07	
8	S20-100×5-B	101×5.05×300	–	202,100	435	7.0	21.5	1348	1268	1.06	
9	S20-150×3-A	151×2.85×450	–	192,600	268	6.8	21.5	1035	966	1.07	
10	S20-150×3-B	152×2.85×450	–	192,600	268	6.8	21.5	1062	966	1.10	
11	S20-150×5-A	150×4.80×450	–	192,200	340	5.6	21.5	1804	1575	1.15	
12	S20-150×5-B	150×4.80×450	–	192,200	340	5.6	21.5	1798	1575	1.14	
13	S30-50×2-A	51×1.81×150	–	205,100	353	10.4	34.9	268	223	1.20	
14	S30-50×2-B	51×1.81×150	–	205,100	353	10.4	34.9	274	223	1.23	
15	S30-50×3-A	51×2.85×150	–	207,900	440	8.2	34.9	394	388	1.02	
16	S30-50×3-B	51×2.85×150	–	207,900	440	8.2	34.9	393	388	1.01	
17	S30-100×3-A	101×2.85×300	–	195,700	358	8.3	34.9	765	770	0.99	
18	S30-100×3-B	100×2.85×300	–	195,700	358	8.3	34.9	742	770	0.96	
19	S30-100×5-A	101×5.05×300	–	202,100	435	7.0	34.9	1434	1323	1.08	
20	S30-100×5-B	101×5.05×300	–	202,100	435	7.0	34.9	1461	1323	1.10	
21	S30-150×3-A	152×2.85×450	–	192,600	268	6.8	34.9	1074	1212	0.89	
22	S30-150×3-B	152×2.85×450	–	192,600	268	6.8	34.9	1209	1212	1.00	
23	S30-150×5-A	150×4.80×450	–	192,200	340	5.6	34.9	1947	1709	1.14	
24	S30-150×5-B	151×4.80×450	–	192,200	340	5.6	34.9	1976	1709	1.16	
25	SHS1C40	150.5×5.83×450	5.3	194,000	497	3	46.6	2768	2681	1.03	[7]
26	SHS1C60	150.6×5.83×450	5.3	194,000	497	3	61.9	2972	2964	1.00	
27	SHS1C80	150.5×5.84×450	5.3	194,000	497	3	83.5	3020	3195	0.95	
28	SHS2C40	150.5×2.78×450	4.6	189,000	448	4	46.6	1382	1490	0.93	
29	SHS2C60	150.5×2.78×450	4.6	189,000	448	4	61.9	1620	1749	0.93	
30	SHS2C80	150.6×2.78×450	4.6	189,000	448	4	83.5	1851	2116	0.87	
31	SHS-2-C30	100×2.2×300	–	202,500	385	12.4	30	534	558	0.96	[8]
32	SHS-2-C60	100×2.0×300	–	202,500	385	12.4	53	687	747	0.92	
33	SHS-2-C100	100×2.2×300	–	202,500	385	12.4	74	836	913	0.92	
34	SHS-5-C30	100×5.0×300	–	180,000	458	3.7	30	1410	1328	1.06	
35	SHS-5-C60	100×4.9×300	–	180,000	458	3.7	53	1488	1397	1.07	
36	SHS-5-C100	100×4.9×300	–	180,000	458	3.7	74	1559	1553	1.00	

The p-ε curves at different points for the specimen are presented in Fig. 10. As expected, values of p near the corner region (Points 1 and 2) are much higher than those at the points away from the corner (Points 3, 4 and 5), which indicates that much stronger confinement is provided by the square steel tube at the corners. Since the interaction stresses at Point 5 are very minor, no p–ε curve is given in Fig. 10 for Point 5. After comparing the interaction stresses at different points for the stainless steel and carbon steel CFST columns, it can be found that the interaction stresses in the CFSST columns are slightly higher. But this difference is very minor, leading to the close N–ε curves of concrete for the two types of columns, as shown in Fig. 8.

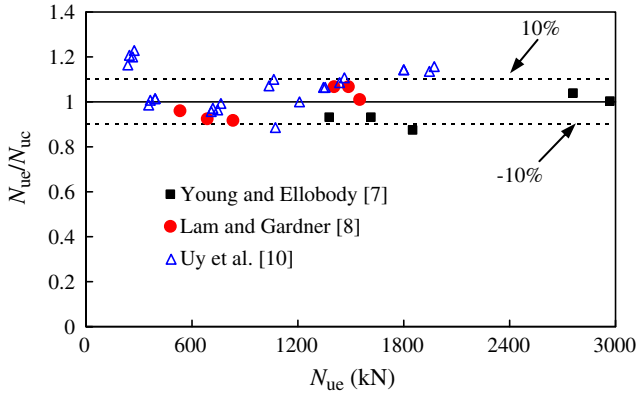

Fig. 7. Comparison between predicted and experimental ultimate strength.

4. Parametric analysis

A parametric study is carried out to investigate the behaviour of CFSST columns. The basic parameters of the columns used in the analysis are: $B=200$ mm, $t=4$ mm, $L=600$ mm, $r_i=4$ mm, $f_c'=30$ MPa, $\sigma_{0.2}=300$ MPa, $n=6$, $E_0=200{,}000$ MPa.

4.1. Effect of grade of stainless steel

Currently, there are various grades of stainless steels for engineers to choose. This variation is generated through the variation in chemical composition and heat treatment of stainless steels. Three types of stainless steels are recommended in Eurocode 3 [32] for structural applications, including ferritic steels, austenitic steels and duplex (austenitic–ferritic) steels. Each type of stainless steel includes several grades. To investigate the effect of grade of stainless steel on N–ε curves, four typical stainless steel grades specified in [32] are selected, which include one ferritic (EN 1.4003), two austenitic (EN 1.4301 and EN1.4401) and one duplex (EN 1.4462) as shown in Table 2.

The N–ε curves of composite columns consisted of different stainless steel grades are depicted in Fig. 11. Since $\sigma_{0.2}$ are different for various stainless steel grades, the load responses in Fig. 11 are normalised with the corresponding predicted peak loads (N_{uc}). From the comparsion, it can be found that the shape of an N–ε curve is mainly affected by $\sigma_{0.2}$ rather than by E_0 or n. This can be explained by the fact that the variation of the specified E_0 or n is not significant. In Eurocode 3 (2006), the range specified for E_0 is 195,000 MPa to 220,000 MPa, and that for n is 5 to 9. When E_0 increases from 195,000 MPa to 220,000 MPa and the other parameters remain the

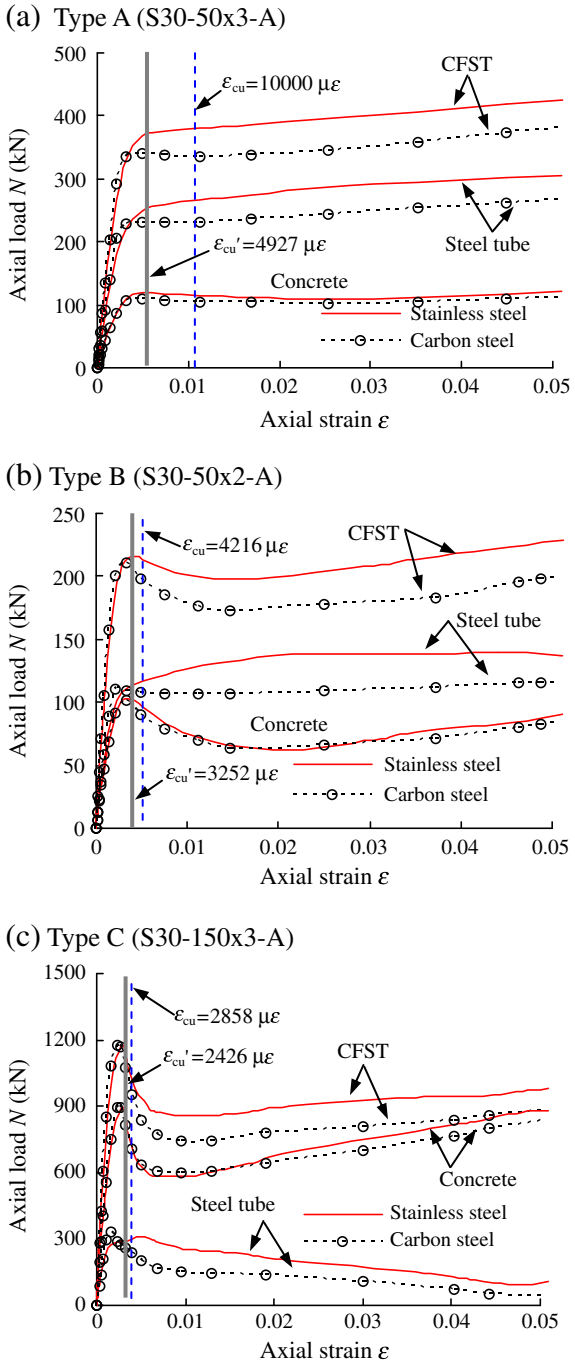

Fig. 8. Comparison of N–ε curves between stainless steel and carbon steel CFST columns.

same, a strength increase of 1.5% is obtained. Likewise, the strength increase is only 0.53% when n increases from 5 to 9. From the analysis, it is concluded that the influence of E_0 and n on the shape of the N–ε curve and the ultimate strength can be ignored.

4.2. Effect of initial imperfections

Generally, initial imperfections have more significant influence on thin-walled tubes than on stocky sections. For CFST columns, the impact of initial imperfections can be reduced by the concrete infill according to [20]. The effect of initial imperfections was analysed and compared for CFSST columns with a B/t ratio of 100, as shown in Fig. 12. The reference column without initial imperfections has a

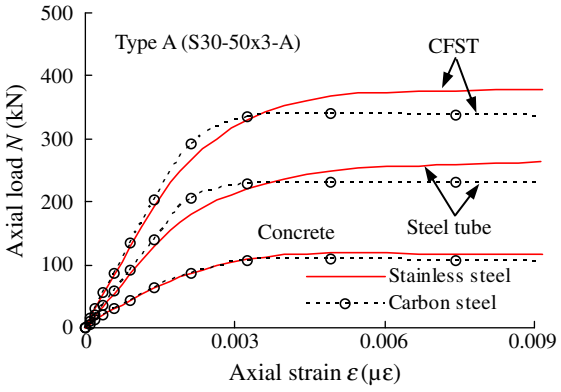

Fig. 9. Initial N–ε curves of stainless steel and carbon steel CFST columns.

predicted peak load of 1619.0 kN, while the predicted strengths for the columns with an imperfection magnitude ω_0 calculated from Eq. (17) and that of 0.01B are 1620.7 kN and 1639.7 kN, respectively. The slightly increased strength of the column with a larger ω_0 is owing to the increased confinement on concrete from the pinching effect of the buckled tube. As can also be seen in Fig. 12, the ultimate strain corresponding to the peak load increases slightly after the initial imperfections are taken into account. From the above comparison, it can be concluded that CFSST columns are not sensitive to the presence of initial imperfections. This is consistent to the results reported earlier by Tao et al. [20] for carbon steel CFST columns. It should be pointed out that this does not mean that a thin-walled CFST column is not affected by initial imperfections. Actually, the out-of-plane deformation of the steel tube caused by the interaction stress plays a similar role as the initial imperfections. Therefore, initial imperfections may not be necessary to be included in FE models for CFSST stub columns.

4.3. Effect of enhanced strength corner properties on ultimate strength

Fig. 13 demonstrates the effect of enhanced strength corner properties of stainless steel on the ultimate strength (N_{uc}) of CFSST columns. As expected, N_{uc} will increase if the enhanced strength at corners is considered. However, the strength enhancement decreases with increasing B/t ratio. This can be explained by two facts: (1) The ultimate strain of the composite column decreases with increasing B/t ratio, leading to the less effectiveness of the utilisation of stainless steel, and (2) the strength contribution of the steel tube decreases when the B/t ratio increases. In the analysed examples, the strength enhancement increases from 4.2% to 15.8% when the B/t ratio

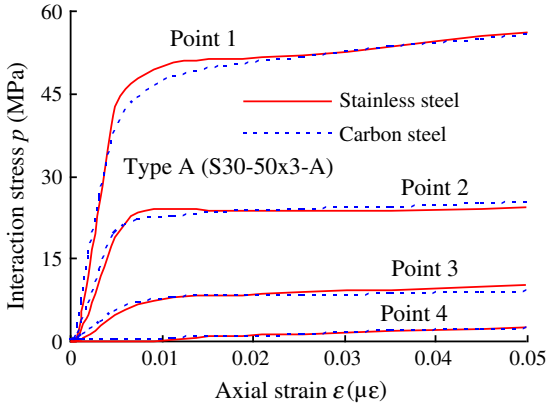

Fig. 10. Comparison of interaction stresses p between stainless steel and carbon steel CFST columns.

Table 2
Mechanical properties for selected stainless steel grades [32].

Type of stainless steel	Grade	$\sigma_{0.2}$ (MPa)	E_0 (MPa)	n
Ferritic	1.4003	280	220,000	7
Austenitic	1.4301	230	200,000	6
Austenitic	1.4401	240	200,000	7
Duplex	1.4462	480	200,000	5

decreases from 40 to 20. Therefore, to consider the effect of enhanced strength corner properties is important for CFSST stub columns with very compact sections.

Currently available cold-formed tubes range from about 0.5t to 3t in internal radius (r_i) of corners. It was found that N_{uc} increases slightly with an increase in r_i. For columns with a B/t ratio of 40, the strength increase is 2.6% as r_i increases from 0.5t to 3t; whilst an increase of 1.6% is obtained for columns with a B/t ratio of 80. When r_i increases, the concrete strength increases as well owing to the higher confinement provided by the steel tube. Meanwhile, the total area of corner regions with strength enhancement for the steel tube will also increase. The beneficial influence, however, is partially counteracted by the reduce of the total area of flat regions of the steel tube and the decrease in $\sigma_{0.2,c}$. In general, the influence of r_i on N_{uc} is not significant. In the following analysis, the r_i/t ratio is taken as unity.

4.4. Effect of concrete strength (f_c')

Due to the uneven distribution of p around the perimeter of the concrete core in a square CFSST column, average interaction stresses p_{ave} at the mid-height are used in the following to evaluate the interaction between the steel tube and concrete. Fig. 14 (a) presents the effect of concrete strength (f_c') on p_{ave}. Obviously, the interaction between the steel tube and concrete is postponed as f_c' increases. This is owing to the fact that higher strength concrete exhibits less lateral expansion at the initial loading stage. For this reason, p_{ave} at the peak load deceases with increasing f_c'. The corresponding p_{ave} are 1.61 MPa, 1.31 MPa and 0.73 MPa for the columns with a concrete strength of 30 MPa, 50 MPa and 80 MPa, respectively. After the peak load is reached, p_{ave} increases slightly with an increase in f_c'. But this delayed increase in passive confinement is not enough to keep high-strength concrete ductile under compression. Thus, the efficiency of the confinement from the same steel tube reduces with increasing f_c'.

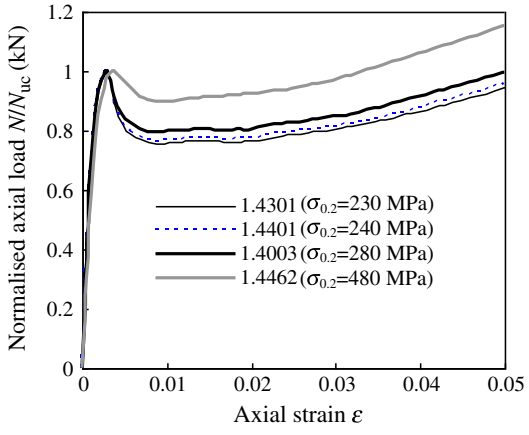

Fig. 11. Effect of grade of stainless steel.

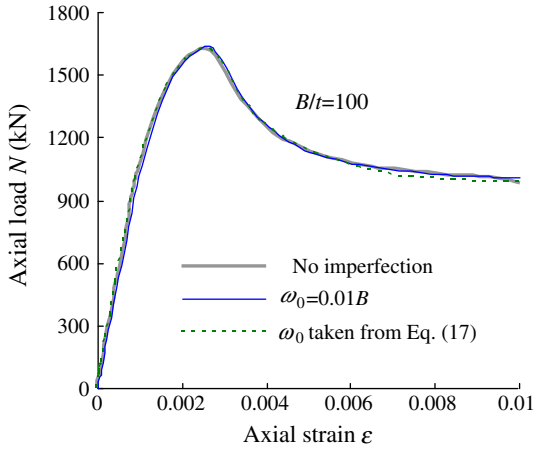

Fig. 12. Effect of initial imperfections on the N–ε curve.

4.5. Effects of steel strength ($\sigma_{0.2}$) and width to thickness (B/t) ratio

Fig. 14(b) and (c) shows the effects of the stainless steel strength ($\sigma_{0.2}$) and B/t ratio of the steel tube on p_{ave}, respectively. p_{ave} increases with increasing $\sigma_{0.2}$ or decreasing B/t ratio, indicating the increasing confinement of the steel tube on the concrete. As $\sigma_{0.2}$ increases or B/t ratio decreases, the N–ε curve of the composite column shows a less pronounced strain-softening behaviour or even demonstrates considerable strain-hardening in the plastic regime. This results not only from the increased contribution of the steel tube, but also from the enhanced confinement on the concrete core.

Fig. 15 shows the effect of B/t ratio on the axial loads carried by the steel tube (N_s), concrete (N_c) and CFSST (N_{uc}) at ultimate state. To make meaningful comparisons, the axial loads are normalised with respect to their corresponding nominal strengths. For the CFSST column, the nominal strength N_0 is defined as follows:

$$N_0 = A_s\sigma_{0.2} + A_c f_c' \tag{18}$$

where the first term and second term in the right hand side of the above equation are the nominal strengths for the steel tube and concrete, respectively.

As can be seen in Fig. 15, N_{uc}/N_0 decreases with increasing B/t ratio. When B/t ratio is close to or larger than 80, N_{uc} is close to but slightly smaller than N_0. For the steel tube, obvious strength enhancement can be observed while the section is very compact. When B/t ratio is larger than 30, the normalised strength of the steel tube [$N_s/(A_s\sigma_{0.2})$] is less

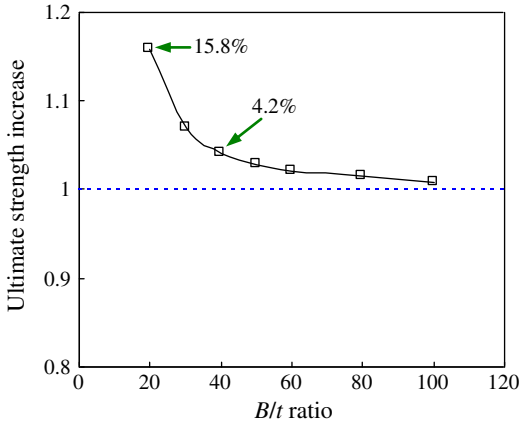

Fig. 13. Effect of enhanced strength corner properties on ultimate strength N_{uc}.

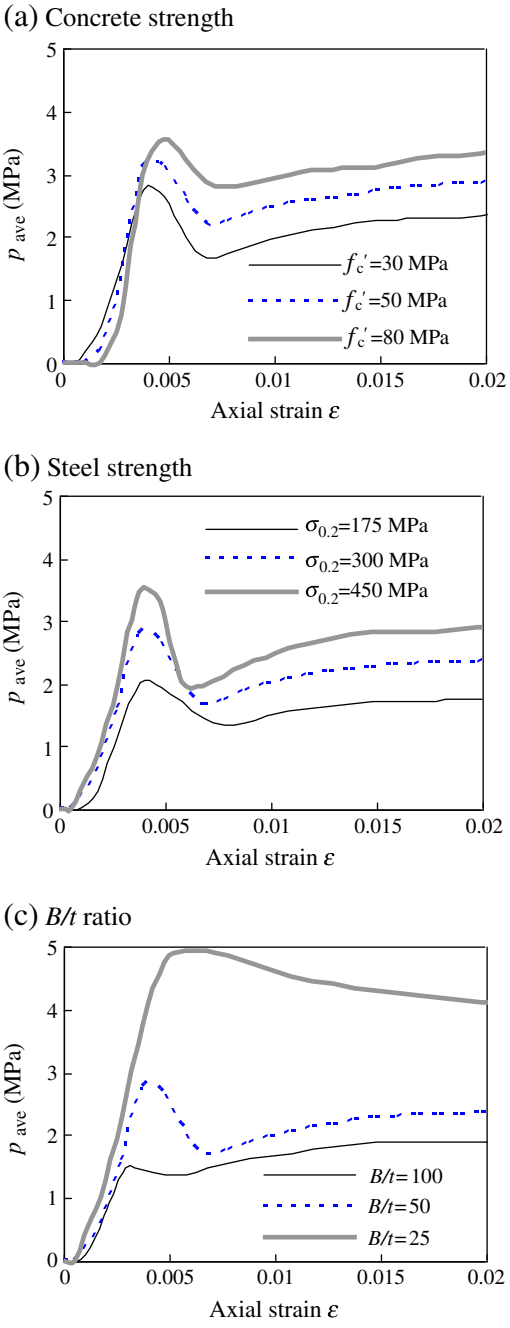

Fig. 14. Effects of different parameters on p_{ave}.

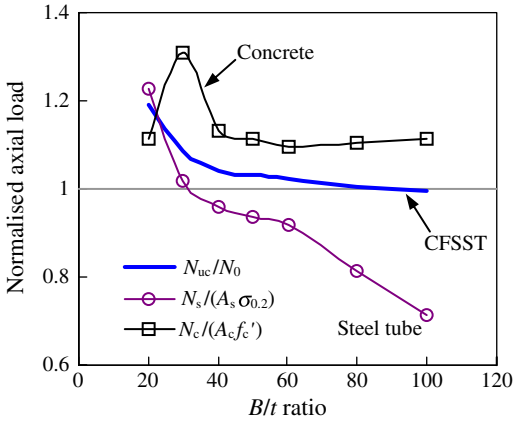

Fig. 15. Effect of B/t ratio on the axial loads carried by different components.

4.6. Classification of N–ε curves

As mentioned earlier, the N–ε curves of CFSST stub columns can be classified into three different groups. If a suitable classification method can be put forward, it will help engineers to design after considering the functional requirements of structures. It is worth noting that the residual strengths of CFSST columns increase somehow after experiencing relatively large axial deformation shown in Fig. 17. This is owing to the strong strain-hardening of stainless steel. Therefore, it is hard to distinguish between Type B and Type C curves based on the FE predictions. In this paper, if the strength at an axial strain of 0.05 for an N–ε curve with declining branch is equal to or exceeds the first peak load, it is classified as Type B curve. Otherwise, it is recognised as Type C curve.

According to the parametric analysis, three main factors, including the concrete strength, stainless steel strength and B/t ratio, determine the shape of the N–ε curve for a CFSST column. For square carbon steel CFST stub columns, Han et al. [33] proposed that the aforementioned confinement factor ξ could be used to distinguish N–ε curves. When ξ is larger than 4.5, the curve is of strain-hardening type. Otherwise, the curve has obvious descending branch. Since the steel ratio α is an equivalent parameter to reflect the influence of B/t ratio, ξ is considered to be a comprehensive index reflecting the composite action between the steel tube and concrete affected by the material strengths and B/t ratio. Generally, the higher the ξ, the more ductile the composite column is.

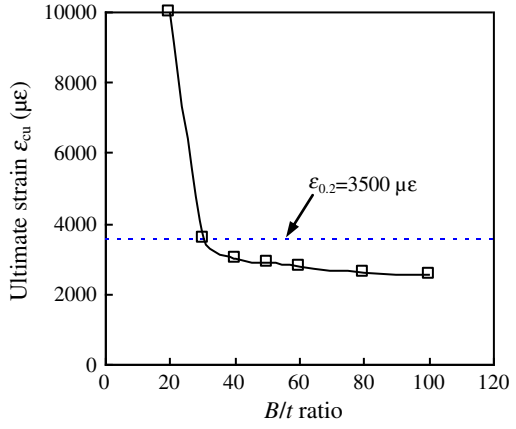

Fig. 16. Ultimate strain as a function of B/t ratio.

than unity. This can be explained by the development of the ultimate strain (ε_{cu}) shown in Fig. 16. Owing to the gradual yielding behaviour of stainless steel, ε_{cu} is smaller than the nominal yield strain ($\varepsilon_{0.2}$) of the steel when B/t ratio is larger than 30. Rapid decline of the curve for the steel tube is observed in Fig. 15 while B/t ratio is larger than 60. This is owing to the significantly increased local buckling effect. As far as the concrete is concerned, the normalised strength $[N_c/(A_cf_c')]$ is always bigger than unity, indicating clear confinement from the steel tube. In this figure, the concrete strength of the column with a B/t ratio of 20 is smaller than that of the column with a B/t ratio of 30. This is owing to the fact that the ultimate strength of the former is achieved with a larger ultimate strain of 10,000 με. In this case, the strength decline is associated with the strain-softening behaviour of concrete, as shown in Fig. 8(a).

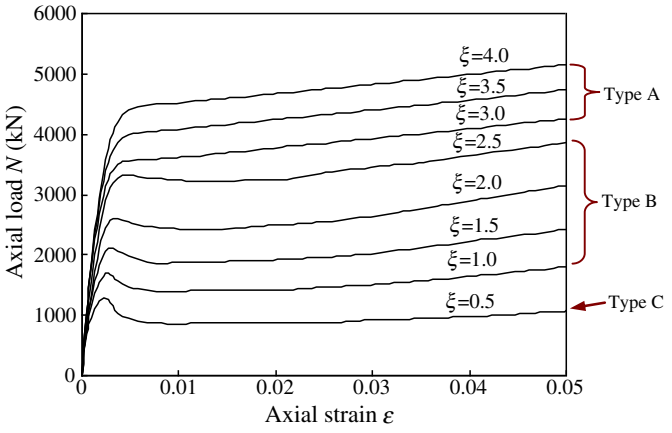

Fig. 17. N–ε curves with different ξ.

Based on the parametric study and the above discussion, it is postulated that ξ can also be used to classify N–ε curves for CFSST columns. For stainless steel, $\sigma_{0.2}$ is used to replace f_y to calculate ξ:

$$\xi = \frac{A_s \cdot \sigma_{0.2}}{A_c \cdot f_{ck}} = \alpha \cdot \frac{\sigma_{0.2}}{f_{ck}} \tag{19}$$

Fig. 17 shows the calculated N–ε curves of typical CFSST columns with different ξ. As ξ increases, the shape of the N–ε curve changes from Type C to Type B and then to Type A.

A total of 65 CFSST columns with ξ ranged from 0.11 to 5.4 are analysed to distinguish different curve types. The obtained results are summarised in Fig. 18. A curve can be recognised as Type A when $\xi \geq 3.0$, and the corresponding curve is Type B when $1.0 \leq \xi < 3.0$. Otherwise, Type C curve is obtained if $\xi < 1.0$. Compared with carbon steel CFST columns, CFSST columns have a smaller ξ limit of 3.0 to retain strain-hardening behaviour owing to the utilisation of the stainless steel material. The ξ limit of the former is 4.5 as mentioned earlier.

5. Load-carrying capacity prediction

At this moment, there is no specific code available to design CFSST columns. Therefore, design equations recommended in several widely used design codes for carbon steel CFST columns are applied to calculate the section capacities of square CFSST stub columns. Compared with the FE predicted strengths, the feasibility of the existing codes in designing CFSST columns can be evaluated. Eighty four numerical examples with parameters selected to cover the practical ranges and conditions are used in the comparisons. The parameters of the examples are: $f_c' = 20$–80 MPa, $\sigma_{0.2} = 175$–450 MPa, $B/t = 20$–100. It should be noted that the obtained ultimate strength of a Type A curve in the numerical examples is determined by ε_{cu} calculated from Eq. (20).

5.1. Existing design codes

Four different design methods are used in this section, which are presented in the American codes ACI [34] and AISC [35], Chinese code DBJ/T [36], and Eurocode 4 [37], respectively. More details of the design equations can be found in Tao et al. [38]. In the calculations, the yield strength f_y has been taken equal to the material 0.2% proof strength $\sigma_{0.2}$.

Fig. 19 compares the FE predicted strengths (N_{uc}) with the calculated strengths based on different code provisions, where N_{ACI}, N_{AISC}, $N_{DBJ/T}$ and N_{EC4} represent the predicted results using ACI [34], AISC [35], DBJ/T [36] and Eurocode 4 [37], respectively. All codes give conservative predictions for CFSST columns with a comparatively large confinement ratio. This is owing to the fact that the strain hardening effect of stainless steel and corner effect are not considered in these codes. Meanwhile, all predictions exhibit a considerable amount of scatter. DBJ/T gives the best predictions with an average value of 1.030 for the ratio of $N_{uc}/N_{DBJ/T}$ and a standard deviation of 0.039. From the comparisons shown in Fig. 19, it seems that more rational design method may be put forward to predict the section capacities of square CFSST stub columns.

5.2. Simplified model

In this paper, the ultimate state for Type B or Type C columns is defined as the instant when the maximum or the first peak load is reached. But for Type A curves, the definition of the ultimate state is not so straightforward since there is no softening branch. In [10], a rather arbitrary definition corresponding to an axial strain of 10,000 με was used. In this paper, an equation to predict the ultimate strains (ε_{cu}) for Type B and Type C columns will be put forward. Afterwards, this equation can be used to define the ultimate state for Type A columns.

A parametric analysis demonstrates that ε_{cu} is mainly affected by the confinement factor ξ and the concrete strength f_c', as shown in Fig. 20. Based on a regression analysis, a simple model is proposed as follows to predict ε_{cu}:

$$\varepsilon_{cu} = 1850 + 13 f_c' + (500 + 4.7 f_c')\xi^{1.35} \tag{20}$$

where the units for ε_{cu} and f_c' are με and MPa, respectively. The calculated values of ε_{cu} using Eq. (20) agree well with the numerical results, as shown in Fig. 20.From Fig. 15, it is postulated that Eq. (18) with suitable modifications may be used to calculate the section

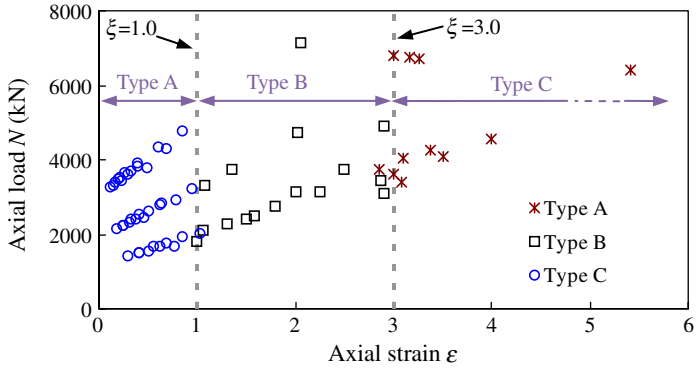

Fig. 18. Classification of N–ε curves by using ξ.

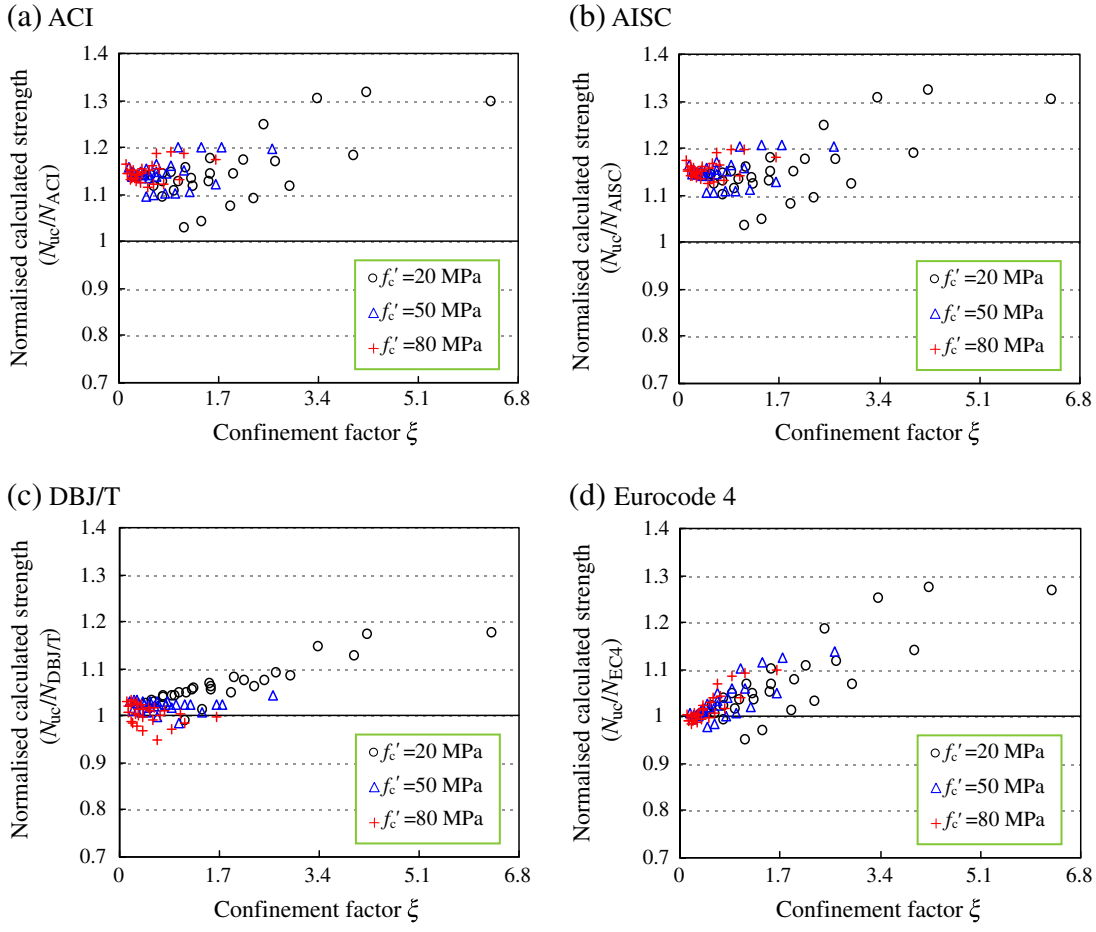

Fig. 19. Comparison between N_{uc} and code predictions.

capacities of square CFSST columns. Actually, Eq. (18) also represents the Eurocode 4 model in predicting the ultimate strengths shown in Fig. 19(d). The modified equation is proposed to take the following form:

$$N_u = kA_s\sigma_{0.2,a} + A_c f_c' \tag{21}$$

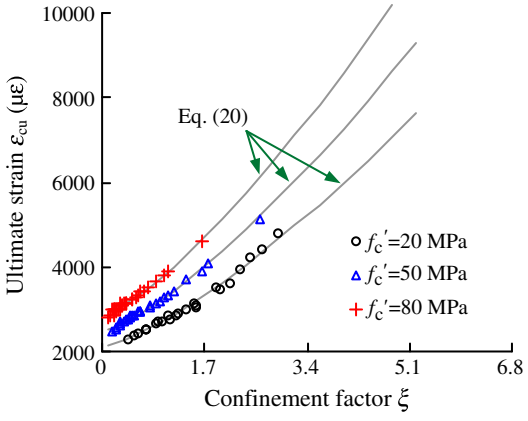

Fig. 20. Effects of ξ and f_c' on ε_{cu}.

in which k is a coefficient representing the influence of nonlinearity and strain hardening of stainless steel, and $\sigma_{0.2,\,a}$ is the average nominal yield strength of the steel tube. $\sigma_{0.2,\,a}$ can be determined as follows:

$$\sigma_{0.2,a} = C\sigma_{0.2,c} + (1-C)\sigma_{0.2,v} \tag{22}$$

where $\sigma_{0.2,\,c}$ is the 0.2% proof stress of the corner material, and can be calculated using Eq. (15); C is the ratio of the total area of corner regions with strength enhancement to the total cross-sectional area of the steel tube.

Based on regression analysis, it was found that k in Eq. (21) is mainly dependent on ξ, and can be expressed as:

$$k = 0.946 + 0.021\xi. \tag{23}$$

To simplify the calculation of N_u, A_s and A_c may be determined by ignoring the existence of the rounded corners since the internal radius of the corners is generally very small.

The comparison between the calculated strengths (N_u) using Eq. (21) and numerical results (N_{uc}) is shown in Fig. 21. A mean value (N_{uc}/N_u) of 1.003 is obtained with a standard deviation of 0.016. Clearly, the agreement between N_u and N_{uc} is quite good.

6. Conclusions

This paper is concerned with the nonlinear analysis of concrete-filled square stainless steel stub columns under axial compression.

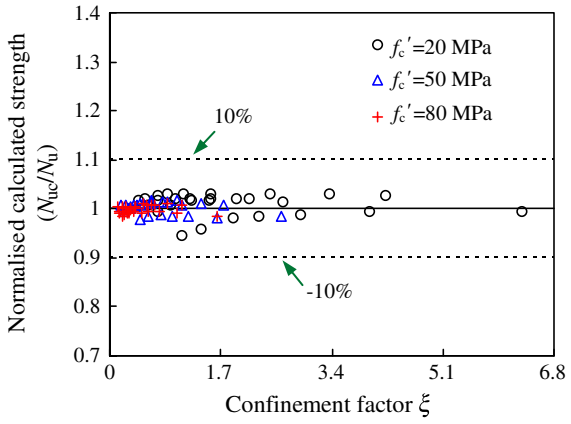

Fig. 21. Comparison of section capacities between Eq. (21) (N_u) and FE predictions (N_{uc}).

The following conclusions can be drawn based on the results of this study:

(1) Finite element modelling of square CFSST columns under axial compression was performed in this paper, in which nonlinear material behaviour, enhanced strength corner properties of steel, and initial geometric imperfections were all included. Close agreement was achieved between the test and FE results in terms of load-deformation response and ultimate strength.
(2) The increased ultimate strength and ductility of a square CFSST stub column compared with its carbon steel counterpart is mainly due to the contribution of the stainless steel tube, which shows a remarkable strain-hardening characteristics.
(3) The confinement factor ξ can be used to gauge the performance of square CFSST stub columns. A classification method based on ξ was put forward to distinguish different types of square CFSST stub columns.
(4) Based on a regression analysis, simplified formulae were proposed for the calculation of the ultimate strains and load-carrying capacities of square CFSST stub columns.

Acknowledgements

This work is supported by the Australian Research Council (ARC) under its Future Fellowships scheme (project no: FT0991433). It has also been partially supported by the Research Grant Scheme and the Eminent Research Visitors Scheme provided by the University of Western Sydney. The financial support is gratefully acknowledged.

References

[1] Mann AP. The structural use of stainless steel. Struct Eng 1993;71(4):60–9.
[2] Gardner L. The use of stainless steel in structures. Prog Struct Eng Mater 2005;7(2):45–55.
[3] Uy B. Stability and ductility of high performance steel sections with concrete infill. J Constr Steel Res 2008;64(7–8):748–54.
[4] Gardner L, Cruise RB, Sok CP, Krishnan K, Ministro J. Life-cycle costing of metallic structures, Engineering Sustainability. Proc ICE 2007;160(4):167–77.
[5] Uy B, Patil SB. Concrete filled high strength steel box columns for tall buildings: behaviour and design. Struct Des Tall Build 2006;5(2):75–94.
[6] Zhao XL, Han LH, Lu H. Concrete-filled tubular members and connections. London: Spon Press; 2010.
[7] Young B, Ellobody E. Experimental investigation of concrete-filled cold-formed high strength stainless steel tube columns. J Constr Steel Res 2006;62(5):484–92.
[8] Lam D, Gardner L. Structural design of stainless steel concrete filled columns. J Constr Steel Res 2008;64(11):1275–82.
[9] Dabaon MA, El-Boghdadi MH, Hassanein MF. Experimental investigation on concrete-filled stainless steel stiffened tubular stub columns. Eng Struct 2009;31(2):300–7.
[10] Uy B, Tao Z, Han LH. Behaviour of short and slender concrete-filled stainless steel tubular columns. J Constr Steel Res 2011;67(3):360–78.
[11] Uy B. Strength of short concrete filled high strength steel box columns. J Constr Steel Res 2001;57(2):113–34.
[12] Roufegarinejad A, Uy B, Bradford MA. Behaviour and design of concrete filled steel columns utilizing stainless steel cross sections under combined actions. Proceedings of the 18th Australian Conference on the mechanics of Structures and materials, Perth, Australia; 2004. p. 159–65.
[13] Ellobody E, Young B. Design and behaviour of concrete-filled cold-formed stainless steel tube columns. Eng Struct 2006;28(5):716–28.
[14] Standards Australia. Cold-formed stainless steel structures. AS/NZS 4673; 2001. Sydney (Australia).
[15] Ellobody E. Nonlinear behavior of concrete-filled stainless steel stiffened slender tube columns. Thin-Walled Struct 2007;45(3):259–73.
[16] Hassanein MF. Numerical modeling of concrete-filled lean duplex slender stainless steel tubular stub columns. J Constr Steel Res 2010;66(8–9):1057–68.
[17] Rasmussen KJR. Full-range stress-strain curves for stainless steel alloys. J Constr Steel Res 2003;59(1):47–61.
[18] ABAQUS. ABAQUS standard user's manual, version 6.9. Providence, RI (USA): Dassault Systèmes Corp.; 2009.
[19] Han LH, Yao GH, Tao Z. Performance of concrete-filled thin-walled steel tubes under pure torsion. Thin-Walled Struct 2007;45(1):24–36.
[20] Tao Z, Uy B, Han LH, Wang ZB. Analysis and design of concrete-filled stiffened thin-walled steel tubular columns under axial compression. Thin-Walled Struct 2009;47(12):1544–56.
[21] Gardner L, Nethercot DA. Experiments on stainless steel hollow sections—part 1: material and cross-sectional behaviour. J Constr Steel Res 2004;60(9):1291–318.
[22] Quach WM, Teng JG, Chung KF. Three-stage full-range stress–strain model for stainless steels. J Struct Eng, ASCE 2008;134(9):1518–27.
[23] Rasmussen KJR, Burns T, Bezkorovainy P, Bambach MR. Numerical modelling of stainless steel plates in compression. Research Report No. R813. Sydney (Australia): Department of Civil Engineering, the University of Sydney; 2002.
[24] Abdel-Rahman N, Sivakumaran KS. Material properties models for analysis of cold-formed steel members. J Struct Eng, ASCE 1997;123(9):51–74.
[25] Ashraf M, Gardner L, Nethercot DA. Strength enhancement of the corner regions of stainless steel cross-sections. J Constr Steel Res 2005;61(1):37–52.
[26] Lecce M, Rasmussen K. Distortional buckling of cold-formed stainless steel sections: finite-element modeling and design. J Struct Eng, ASCE 2006;132(4):505–14.
[27] Gardner L, Nethercot DA. Numerical modeling of stainless steel structural components—a consistent approach. J Struct Eng, ASCE 2004;130(10):1586–601.
[28] Ashraf M, Gardner L, Nethercot DA. Finite element modelling of structural stainless steel cross-sections. Thin-Walled Struct 2006;44(10):1048–62.
[29] Cruise RB, Gardner L. Strength enhancements induced during cold forming of stainless steel sections. J Constr Steel Res 2008;64(11):1310–6.
[30] Ellobody E, Young B. Structural performance of cold-formed high strength stainless steel columns. J Constr Steel Res 2005;61(12):1631–49.
[31] Tao Z, Han LH. Behaviour of concrete-filled double skin rectangular steel tubular beam-columns. J Constr Steel Res 2006;62(7):631–46.
[32] Eurocode 3. Design of steel structures, part 1–4: general rules-supplementary rules for stainless steel. BS EN 1993-1-4: 2006. London (UK): British Standards Institution; 2006.
[33] Han LH, Zhao XL, Tao Z. Tests and mechanics model for concrete-filled SHS stub columns, columns and beam-columns. Steel Compos Struct 2001;1(1):51–74.
[34] ACI Committee 318. Building code requirements for reinforced concrete (ACI 318–08) and commentary. Detroit (USA): American Concrete Institute; 2008.
[35] ANSI/AISC 360–05. Specification for structural steel buildings. Chicago (IL, USA): American Institute of Steel Construction; 2005.
[36] DBJ/T 13-51-2010. Technical specification for concrete-filled steel tubular structures. Fuzhou (China): The Department of Housing and Urban-Rural Development of Fujian Province; 2010 [in Chinese].
[37] Eurocode 4. Design of composite steel and concrete structures, part 1.1, general rules and rules for building. BS EN 1994-1-1: 2004. London (UK): British Standards Institution; 2004.
[38] Tao Z, Han LH, Wang ZB. Experimental behaviour of stiffened concrete-filled thin-walled hollow steel structural (HSS) stub columns. J Constr Steel Res 2005;61(7):962–83.